Pergamon

0956-7151(95)00325-8

Acta mater. Vol. 44, No. 5, pp. 1793–1799, 1996
Elsevier Science Ltd

1359-6454/96 $15.00 + 0.00

DIFFUSION INDUCED RECRYSTALLIZATION OF TiC

KI-WOONG CHAE[1]†, CHEOL SEONG HWANG[1]‡, DOH-YEON KIM[1]§ and SEONG-JAI CHO[2]

[1]Department of Inorganic Materials Engineering, College of Engineering, Seoul National University, Seoul 151-742 and [2]Korea Research Institute of Standards and Science, Taejon 305-606, Korea

(Received 19 April 1995; in revised form 21 August 1995)

Abstract—When large TiC particles (30 μm in average) are embedded in Cr_3C_2 powders and heat-treated at 1550°C, recrystallization occurs from the surface of the TiC particles, and they are finally replaced by an entirely new set of (Ti,Cr)C alloy grains. The observed recrystallization is greatly suppressed when ZrC is added in the Cr_3C_2 matrix. The results are in agreement with the prediction that a lattice mismatch due to the diffusion of Cr and resultant formation of misfit dislocations are the major cause of recrystallization. The diffusion induced recrystallization (DIR) process is observed in detail by using a transmission electron microscope.

1. INTRODUCTION

When solute atoms diffuse into crystals along grain boundaries, it is usually assumed that the equilibration reaction occurs simply by a subsequent symmetrical lattice diffusion. During the diffusion process, however, recent studies with some metallic and oxide systems have demonstrated that the grain boundaries migrate, leaving behind a new solid solution of the initial material and the solute atoms. At the specimen surface where the solute concentration is high enough, recrystallization also occurs by nucleating new alloy grains. The phenomena, generally referred to as diffusion-induced grain boundary migration (DIGM) and diffusion-induced recrystallization (DIR), have been recently reviewed [1–3].

For these diffusion-induced phenomena, particularly those of DIGM, the coherency strain energy which arises in the thin diffusion layer of the receding concave boundary has been suggested as its driving force [4–6]. The diffusion layers tend to adapt to the local change in lattice parameters brought about by a change in composition but they are constrained by the underlying initial crystals, thus creating a coherency strain. Such a coherency strain has been experimentally tested by simultaneously introducing two species of solute atoms which give rise to a compressive and tensile strain, respectively. The DIGM behavior is consistent with the coherency strain which was systematically varied, and, indeed, no boundary migration was observed when the strain was zero [4, 5].

Although the mechanism of DIR is likely to be similar to that of DIGM, it has not yet been thoroughly tested experimentally. Most of the investigations on DIR [6–14] have been rather limited to characterizations of the macroscopic phenomena and detailed nucleation and growth processes have not been reported. Furthermore, DIR has been observed in a number of metallic and oxide systems, but an experimental demonstration in the carbide system has not yet been made. The aim of this study is thus to elucidate the basic mechanisms of DIR using the carbide system. Among various carbides, it is expected that the composition change of TiC can produce a sufficient diffusional strain to induce DIR. In fact, TiC particles in a Mo–Ni [15] or Fe [16] liquid matrix have been shown to develop a very irregular shape as a result of material transfer between the regions within a single grain by coherency strain energy. In this experiment, coarse TiC grains were heat-treated with other carbide powders such as Cr_3C_2 and ZrC. The microstructural evolution of the TiC grains during heat-treatment was observed by optical and transmission electron microscopy (TEM), and a detailed process of DIR is discussed.

2. EXPERIMENTAL PROCEDURE

Very large TiC particles in polyhedral shape (30 μm in average) were used to prepare the specimens of 20TiC–80Cr_3C_2 and 20TiC–74Cr_3C_2–6ZrC (in wt.%). Contents of combined and free carbon of

†Present address: Department of Materials Engineering, College of Engineering, Hoseo University, Asan 336-795, Korea.

‡Present address: Samsung Electronics Co., Ltd., Suwon 449-900, Korea.

§To whom all correspondence should be addressed.

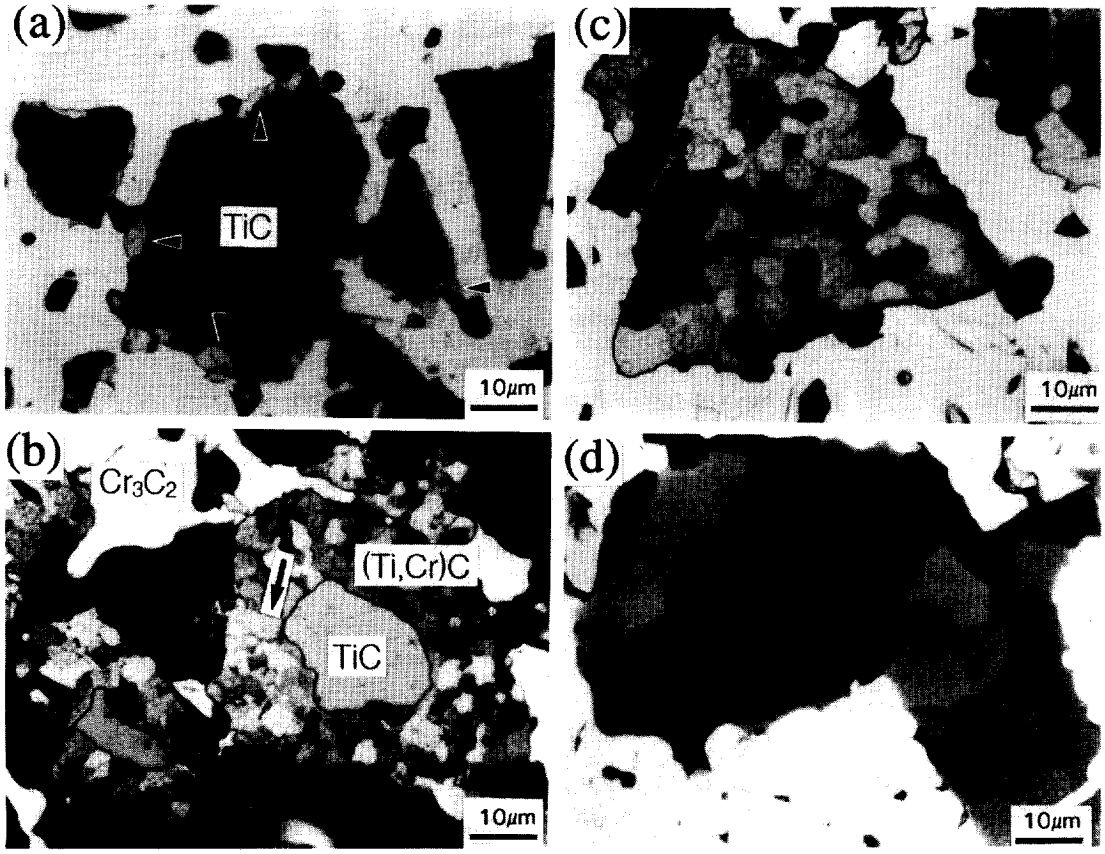

Fig. 1. Microstructures of the TiC–Cr_3C_2 specimen heat-treated at 1550°C for (a) 0 min, (b) 15 min, (c) 1 h, and (d) 8 h.

the TiC powders reported by the producer† were approximately 19.2 and 0.4 wt.%, respectively. The average particle sizes of Cr_3C_2 and ZrC were approximately 2 μm. In order to maintain the large size of TiC particles during processing, the powder mixtures were obtained by hand-mixing. Acetone was added to the mixed powders to make a slurry which was then stirred thoroughly with a glass rod. The powder mixtures were compacted at 30 MPa into cylindrical compacts of 10 mm in diameter. The compacts were then sintered in a vacuum furnace at 1550°C for 0–8 h using a graphite heating element. The heat-treatment for 0 h means that the specimen was cooled immediately after the sintering temperature was reached. The heating rate was 15°C/min and a vacuum of about 13.3 MPa (0.1 torr) was maintained.

Specimens for optical microscopic examinations were finally polished with 0.05 μm alumina powders and etched for 15 s with Murakami's solution (H_2O:NaOH:$K_3Fe(CN)_6$ = 10:1:1). Quantitative microchemical analysis in the TiC grains was carried out using energy dispersive X-ray spectroscopy (EDX). For TEM‡ observation, the specimens heat-treated for 0 and 1 h were ground to 70 μm in thickness and then dimpled down to 5 μm. Ion thinning was carried out using argon ions at 5 kV.

3. RESULTS AND DISCUSSION

3.1. Optical microscopy

Figure 1 shows the microstructural evolution of the TiC particles in the 20TiC–80Cr_3C_2 specimen as a function of the heat-treatment time. Regardless of the heat-treatment time, all specimens exhibit some pores at the vicinity of TiC particles. The coarse TiC particles used in this experiment and consequent imperfections in the packing of starting powders are assumed to be the cause of such poor densification. After heat-treatment for 0 h, [Fig. 1(a)], the coarse TiC particle (dark grey) dispersed in the Cr_3C_2 matrix can be easily discerned. The absence of any grain boundaries in the TiC grains indicates that the coarse TiC particles used are single crystalline. Note, however, that a few (Ti,Cr)C solid solutions have already formed at the peripheries of the TiC particle as indicated by arrows in the figure, which are somewhat fainter than the initial TiC.

The microstructure of the specimen after heat-treatment for 15 min is shown in Fig. 1(b). Although the overall shape of the coarse TiC grains is main-

†Hermann C. Starck Berlin, Goslar, Germany.
‡JEOL 200CX, Philips CM-20.

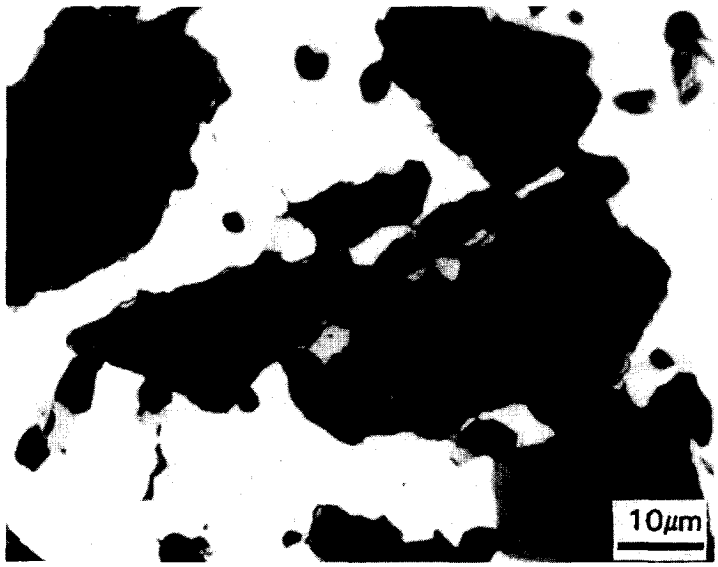

Fig. 2. Microstructure of the 20TiC–74Cr_3C_2–6ZrC specimen heat-treated at 1550°C for 15 min.

tained, the formation of the surrounding region which is composed of fine grains about 1–2 μm in size is noted. EDX analysis of the specimen showed that the surrounding fine grains are (Ti,Cr)C, whereas the inside core is pure TiC. The composition measurement in the surrounding recrystallized region showed that the Cr_3C_2 concentration† decreases from 15 mol% with distance from the original Cr_3C_2/TiC interface. For the recrystallized (Ti,Cr)C grains which are in contact with the TiC core, the Cr_3C_2 concentration was about 5 mol%.

After heat-treatment for 1 h [Fig. 1(c)], all TiC grains, initially single crystals, were completely recrystallized to fine (Ti,Cr)C grains and the pure TiC cores were not observed anymore. The recrystallized grains were uniform in size ($\sim 3\,\mu$m) and they were clearly discerned by their different etching rates depending on the crystallographic orientation. The results may indicate that the grain boundaries of the newly formed (Ti,Cr)C grains at this stage are high-angle grain boundaries. Further heat-treatment resulted in the growth of recrystallized grains. After heat-treatment for 8 h, the average size of the (Ti,Cr)C grains was about 15 μm [Fig. 1(d)].

In cubic crystals such as TiC, the coherency strain energy resulting from a lattice mismatch, which is known to be the driving force of DIGM, can be expressed as [1]

$$G_c = Y(n)\delta^2 \tag{1}$$

where $Y(n)$ is the orientation dependent elastic modulus. The coherency strain δ in the solute diffusion zone is given by

$$\delta = (a_0 - a)/a_0, \tag{2}$$

where a_0 and a are the lattice parameters of solute free crystals and the new solid solution, respectively. DIR was observed to occur when composition change was large and the minimum coherency strain δ required for DIR to occur was estimated to be of the order of 10^{-3}, which is about 10 times larger than that of DIGM [6].

When the thickness of the (Ti,Cr)C layer on TiC reaches a certain critical value, the coherency strain developed in the mixed carbide layer would be relieved by the production of misfit dislocations. The larger the lattice mismatch between the TiC matrix and (Ti,Cr)C diffusion layer, the higher the density of misfit dislocations. It is expected that these misfit dislocations play an important role in bringing about DIR. Note that the recrystallization of plastically deformed metal is the consequence of increased dislocation density.

Goldschmidt [17] reported the following linear equation to describe the lattice parameter of (Ti,Cr)C as a function of Cr_3C_2 content:

$$a = a_0 - 0.006x \tag{3}$$

where a_0 is the lattice parameter of pure TiC and x is the Cr_3C_2 concentration (in mol%) in TiC. Note that the Cr_3C_2 content of the (Ti,Cr)C grains which are in contact with the TiC core was 5 mol%. The value of δ between this (Ti,Cr)C and pure TiC estimated from the above equation was 6.9×10^{-3}, which is of the same order of magnitude as those reported in the DIR of ZrO_2 [6].

Contrary to the lattice parameter of (Ti,Cr)C which decreases with Cr content, the lattice parameter of (Ti,Zr)C is known to increase with Zr content [18]. As a consequence, the addition of ZrC to the Cr_3C_2 matrix may decrease the difference in

†Value calculated from the determined fractio of Ct: Cr/Ti + Cr.

lattice parameters between pure and mixed carbide by forming (Ti,Cr,Zr)C. Therefore, DIR may not occur or may proceed at a slower rate because of its reduced driving force. Figure 2 shows the microstructure of the 20TiC–74Cr_3C_2–6ZrC specimen (in wt%) after heat-treatment at 1550°C for 15 min. Although the heat-treatment condition was the same as that of the specimen shown in Fig. 1(b), DIR was considerably suppressed and TiC grains almost maintained their initial grain shape. This result is in agreement with the prediction of the strain model.

3.2. Transmission electron microscopy

In order to investigate the initial stage of DIR, the TiC particles heat-treated in Cr_3C_2 powder at 1550°C for 0 h have been observed in detail by transmission electron microscopy. Figure 3 is a brightfield TEM micrograph from a region near the surface of a TiC particle, taken with an electron beam close to ⟨112⟩. Two different regions are formed on the surface of the TiC particle: the first is a band-shaped layer with a thickness of about 0.3 μm, indicated by (a), and the other is the region (b) where many stacking faults are formed. Electron diffraction analysis showed that these regions have the same crystal structure to that of TiC. The Cr_3C_2 concentration determined along the line AB was shown in Fig. 4. Between regions (a) and (b), a sharp discontinuity from 6 to 3 mol% was noted.

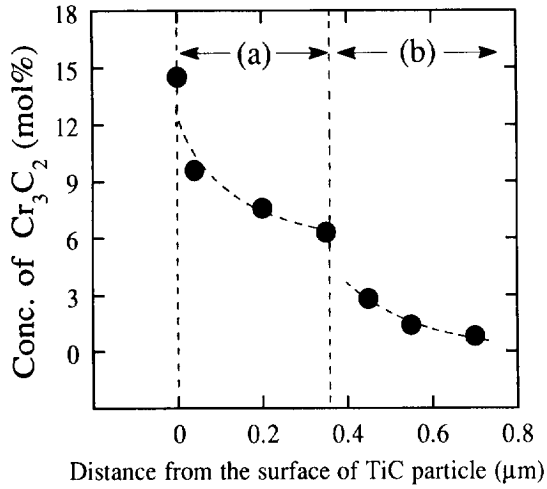

Fig. 4. Composition profile of the recrystallized region for the specimen shown in Fig. 3.

In layer (a), sub-boundaries of dislocation networks (indicated by arrows) and the subgrains of nearly uniform size (less than 0.5 μm and labelled 1–5) were observed. From the selected area diffraction patterns, the misorientations in these subgrains were determined to be very small. The sub-boundary between subgrains 1 and 2 is parallel to the electron beam direction so that it appears as a straight line. Note that subgrains like 2 and 3 exhibit much lower

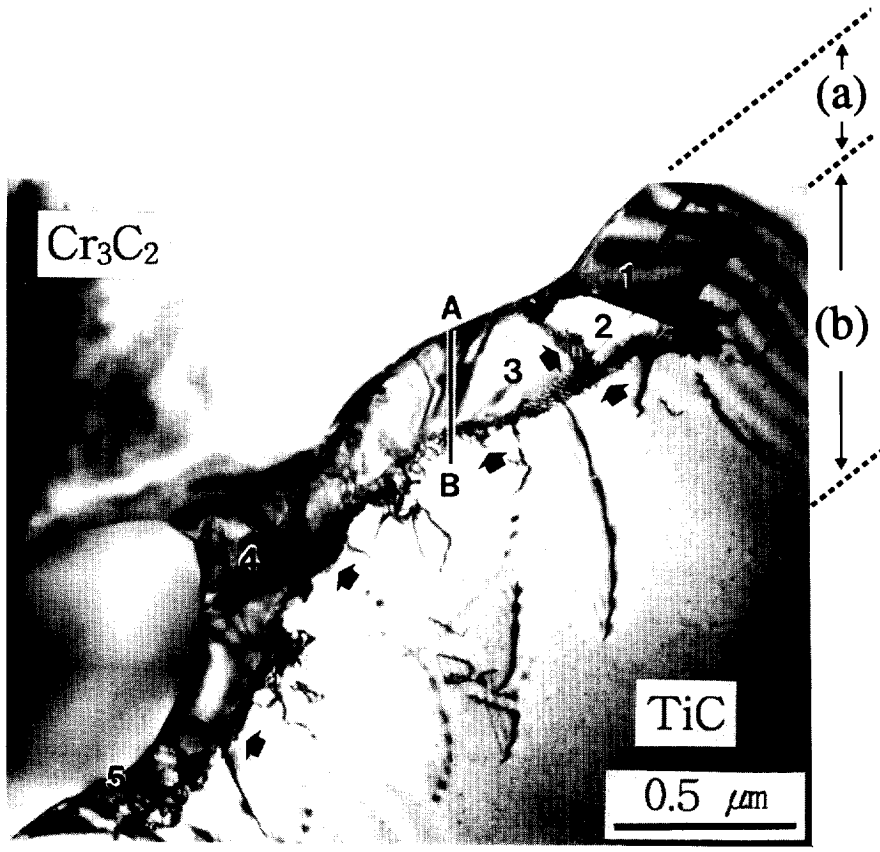

Fig. 3. TEM micrograph of a TiC particle heat-treated with Cr_3C_2 powder at 1550°C for 0 min

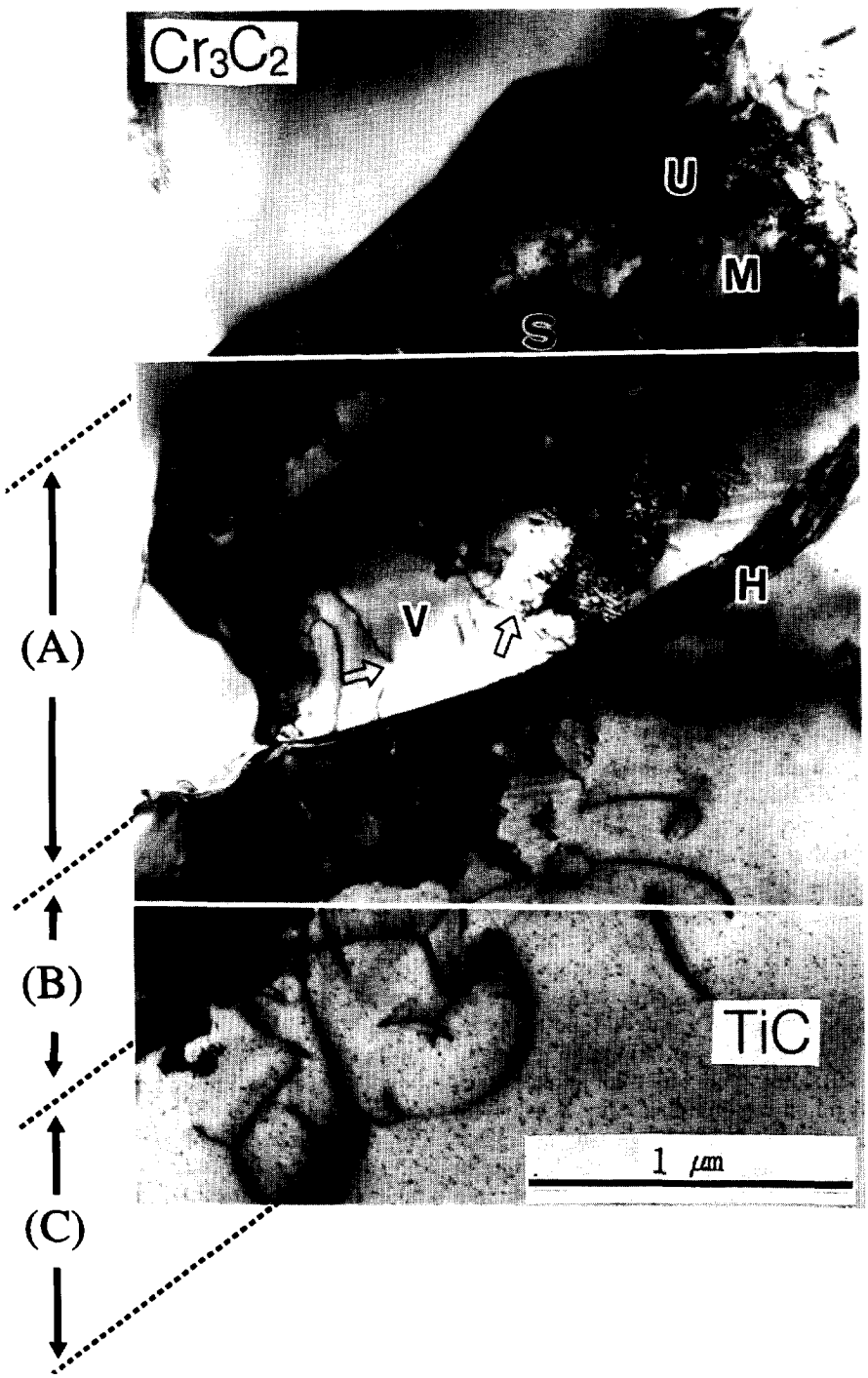

Fig. 5. TEM micrograph of a TiC particle heat-treated with Cr_3C_2 powder at 1550°C for 0 min.

dislocation densities compared to subgrains 4 and 5. From the Cr_3C_2 concentration of region (a), which ranged from 6 to 15 mol% (Fig. 4), the lattice strain induced by Cr diffusion is calculated to be between 8.3×10^{-3} and 2.1×10^{-2} by equation (3). On the other hand, diffusion of Cr into TiC mainly through the sub-boundaries may explain the discontinuity of Cr concentration observed between regions (a) and (b).

In region (b) where the Cr_3C_2 concentration is less than 3 mol%, only stacking faults and associated partial dislocations were observed without any dislocation networks. The lattice strain of this region is calculated to be less than 10^{-3}. Note also that TiC crystal beneath region (b), which is far away from the Cr diffusion does not exhibit any crystal defects. In this respect, the stacking faults are expected to be generated when the concentration of Cr_3C_2 in TiC is

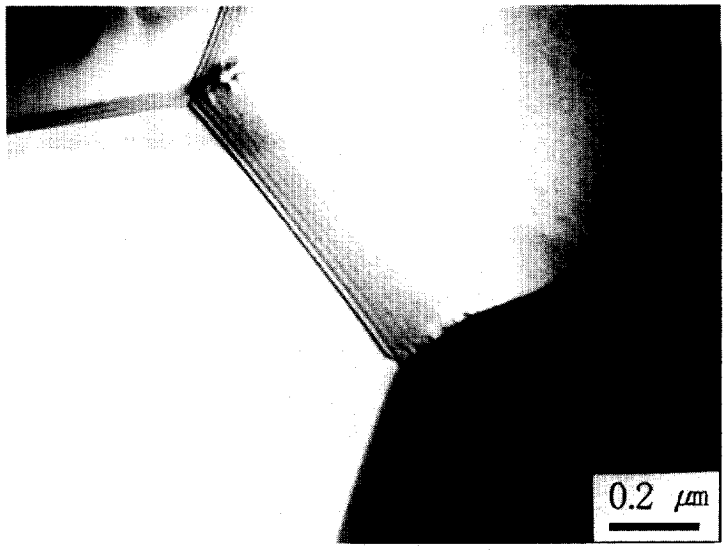

Fig. 6. TEM micrograph of a TiC particle heat-treated with Cr_3C_2 powder at 1550°C for 1 h.

lower than about 3 mol%. Further increase of Cr_3C_2 concentration beyond 6 mol%, for instance, would result in the formation of misfit dislocations. By the analysis in the two beam condition, the Burgers vector of dislocation networks observed in Fig. 3 is determined to be $a/2\langle 110\rangle$ type. A similar network structure was also observed [19, 20] in a TiC single crystal deformed at high temperatures.

Figure 5 is another TEM micrograph from the same specimen, but obtained in the region where the newly formed reaction layer is a little bit thicker than that observed in Fig. 3. In this respect, Fig. 5 is expected to exhibit the microstructural feature of DIR slightly more progressed than that shown in Fig. 3. In the micrograph, three different regions as indicated by (A), (B) and (C) are observed. In region (A), the subgrains containing high dislocation densities (S, U and M), and dislocation free (such as V) are observed. The subgrain such as V is much larger in size than others and also than the subgrains observed in Fig. 3. Misorientation between the subgrains in S, U, M and V were also fairly small. On the other hand, the misorientation between regions (A) and (B), which were divided by the dislocation networks (labelled H), was about 7–8°. Therefore the boundary H is no longer a simple low-angle boundary. It should also be emphasized that regions (B) and (C) of Fig. 5 are very similar to regions (a) and (b) of Fig. 3, respectively. In region (B), which is about 0.3 μm thick, the dislocation networks are observed, and the stacking faults are the main defects in region (C).

These observations demonstrate how the DIR occurs in TiC. After a sufficient amount of Cr diffusion into TiC which results in the generation of misfit dislocations, the sub-boundaries are developed through the rearrangement and annihilation of the misfit dislocations [as observed in region (a) of Fig. 3]. The next stage is the coalescence [21, 22] or the combination of subgrains [23–25], which is believed to occur also by the rearrangement of dislocations. Note that the energy associated with a coalesced grain is less than that associated with two separated grains. Furthermore, the movement of dislocations in terms of either glide or climb is not difficult to understand at this high-temperature. This state may correspond to region (A) of Fig. 5: the subgrain V is expected to be the result of a combination of small subgrains. The traces of sub-boundaries that still remain in grain V (as indicated by arrows) may support the coalescence process.

An extension of this coalescence process will eventually result in a grain separated by a high-angle boundary, as indicated by H in Fig. 5. By the enhanced diffusion of Cr through the boundary H, the initiation of DIR is expected to occur in succession at regions (B) and (C) of Fig. 5. The micrograph taken from a specimen heat-treated at 1550°C for 1 h is given in Fig. 6. Most of the dislocations and stacking faults completely disappeared in the (Ti,Cr)C grains which are separated by high-angle grain boundaries.

4. CONCLUSIONS

During the heat-treatment of TiC particles in the Cr_3C_2 matrix, new solid solution (Ti,Cr)C grains were nucleated and an entirely new set of grains was formed. This diffusion induced recrystallization (DIR) is the first experimental demonstration in carbide materials. Recrystallization was suppressed when ZrC powder was added in the Cr_3C_2 matrix, because the difference in lattice parameters between TiC and the solid-solution carbide was diminished by forming (Ti,Cr,Zr)C. The results hence support the strain energy as a driving force of DIR.

When the lattice strain induced by Cr diffusion exceeds 10^{-3}, the misfit dislocations were generated and hexagonal networks were formed. The subgrains were observed to appear as a result of dislocation rearrangement, and the coalescence of subgrains was expected to lead to the generation of high-angle boundaries. Consequently, the DIR process itself is analogous to the general recrystallization observed in cold-worked metal, for which the driving force comes from the stored energy associated with dislocations created by plastic deformation. In DIR, on the other hand, such dislocations are created by the diffusion of solute atoms which results in the change of lattice parameters.

Acknowledgements—The support from the Korea Ministry of Education, under research grant for advanced materials in 1994 is greatly acknowledged. The comments of Prof. Hu-Chul Lee when reviewing the manuscript are appreciated.

REFERENCES

1. D. N. Yoon, in *Annual Review of Material Science* (edited by R. A. Huggins, J. A. Giordmaine and J. B. Wachman, Jr), Vol. 19, pp. 43–58. Annual Reviews Inc., Palo Alto, CA (1989).
2. C. A. Handwerker, in *Diffusion Phenomena in Thin Films and Microelectronic Materials* (edited by D. Gupta and P. S. Ho), pp. 245–322. Noyes Publications, NJ (1987).
3. A. H. King, *Int. Mater. Rev.* **32,** 173 (1987).
4. W. H. Rhee, Y. D. Song and D. N. Yoon, *Acta metall.* **35,** 57 (1987).
5. W. H. Rhee and D. N. Yoon, *Acta metall.* **37,** 221 (1989).
6. J.-W. Jeong, D. N. Yoon and D.-Y. Kim, *Acta metall.* **39,** 1275 (1991).
7. F. J. A. Den Broeder and S. Nakahara, *Scripta metall.* **17,** 399 (1983).
8. J.-J. Kim, B.-M. Song, D.-Y. Kim and D. N. Yoon, *Am. Ceram. Bull.* **65,** 43 (1986).
9. H.-Y. Lee and S.-J. L. Kang, *Acta metall.* **38,** 1307 (1990).
10. T. A. Parthasarathy and P. G. Shewmon, *Metall. Trans.* **14A,** 2560 (1983).
11. L. Chongmo and M. Hillert, *Acta metall.* **29,** 1949 (1981).
12. F. J. A. Den Broeder, M. Klerk, J. M. Vandenberg and R. A. Hamm, *Acta metall.* **31,** 285 (1983).
13. T. A. Parthasarathy and P. G. Shewmon, *Acta metall.* **32,** 29 (1984).
14. F. S. Chen and A. H. King, *Scripta metall.* **21,** 649 (1987).
15. D.-I. Chun, D.-Y. Kim and K.-Y. Eun, *J. Am. Ceram. Soc.* **76,** 2049 (1993).
16. K.-W. Chae, D.-I. Chun, D.-Y. Kim, Y.-J. Baik and K.-Y. Eun, *J. Am. Ceram. Soc.* **73,** 1979 (1990).
17. H. J. Goldschmidt, in *Interstitial Alloys*, p. 151. Butterworths, London (1967).
18. J. T. Norton and A. L. Mowry, *Metals Trans.* **185,** 133 (1949).
19. G. E. Hollox and R. E. Smallman, *J. appl. Phys.* **37,** 818 (1966).
20. G. Das, K. S. Mazdiyasni and H. A. Lipsitt, *J. Am. Ceram. Soc.* **65,** 104 (1982).
21. J. C. M. Li, *J. appl. Phys.* **33,** 2958 (1962).
22. R. C. Koo and H. G. Sell, in *Recrystallization, Grain Growth and Textures*, pp. 97–98. A.S.M., New York (1965).
23. H. Hu, *Trans. AIME* **224,** 745 (1962).
24. J. O. Stiegler, C. K. H. Dubose, R. E. Reed and C. J. Mchargue, *Acta metall.* **11,** 851 (1963).
25. M. R. Drury and F. J. Humphreys, *Acta metall.* **34,** 2259 (1986).